Journal of Applied Physics

Electronic properties of intrinsic vacancies in single-layer CaF_2 and its heterostructure with monolayer MoS_2

Cite as: J. Appl. Phys. **130**, 055301 (2021); https://doi.org/10.1063/5.0055044
Submitted: 24 April 2021 • Accepted: 07 July 2021 • Published Online: 04 August 2021

Zhenzhen Li, Mehmet Baskurt, Hasan Sahin, et al.

View Online Export Citation CrossMark

ARTICLES YOU MAY BE INTERESTED IN

Calcium fluoride as high-k dielectric for 2D electronics
Applied Physics Reviews **8**, 021307 (2021); https://doi.org/10.1063/5.0036987

Thermoelectric properties of the SnS monolayer: Fully ab initio and accelerated calculations
Journal of Applied Physics **130**, 054301 (2021); https://doi.org/10.1063/5.0058125

Thermoelectric and optical properties of 2D hexagonal Dirac material Be_3X_2 (X=C, Si, Ge, Sn): A density functional theory study
Journal of Applied Physics **130**, 055106 (2021); https://doi.org/10.1063/5.0059942

Lock-in Amplifiers up to 600 MHz
Zurich Instruments
Watch

© 2021 Author(s).

Journal of Applied Physics ARTICLE scitation.org/journal/jap

Electronic properties of intrinsic vacancies in single-layer CaF_2 and its heterostructure with monolayer MoS_2

Cite as: J. Appl. Phys. **130**, 055301 (2021); doi: 10.1063/5.0055044
Submitted: 24 April 2021 · Accepted: 7 July 2021 ·
Published Online: 4 August 2021

View Online Export Citation CrossMark

Zhenzhen Li,[1,a)] Mehmet Baskurt,[2] Hasan Sahin,[2] Shiwu Gao,[1] and Jun Kang[1,a)]

AFFILIATIONS

[1]Beijing Computational Science Research Center, Beijing 100193, China
[2]Department of Photonics, Izmir Institute of Technology, 35430 Izmir, Turkey

[a)]**Authors to whom correspondence should be addressed:** zzli@csrc.ac.cn and jkang@csrc.ac.cn

ABSTRACT

Exploring gate insulator materials for 2D transistors and their defect properties is of importance for device performance optimization. In this work, the structural and electronic properties of intrinsic vacancies in the CaF_2 single layer and its heterostructures with monolayer MoS_2 are investigated from first-principles calculations. V_{Ca} introduces a shallow defect level close to the VBM, whereas V_F introduces a deep level below the CBM. In both cases, spin polarization is observed. Overall, V_F has a relatively lower formation energy than V_{Ca}, except for the extreme Ca-rich case. Thus, V_F should be dominant in CaF_2. The band offset between CaF_2 and MoS_2 is determined to be type-I, with large offsets at both the conduction band and valence band. With the presence of vacancies in CaF_2, the type-I band offset is preserved. The electron or hole on the defect states will transfer from CaF_2 to MoS_2 due to the large band offset, and spin polarization vanishes. Nevertheless, there are no defect states inside the gap or around the band edge of MoS_2, and the electronic properties of MoS_2 are almost intact. Compared with *h*-BN that has a small valence band offset with MoS_2 and could introduce in-gap defect states, CaF_2 can be a good candidate to serve as the dielectric layer of MoS_2-based transistors.

Published under an exclusive license by AIP Publishing. https://doi.org/10.1063/5.0055044

I. INTRODUCTION

Semiconducting transition metal dichalcogenides (TMDs) have been extensively investigated due to their electronic, optical, and mechanical properties[1–5] as well as their combinations with other two-dimensional crystals[6–9] which led to an emergence of a new class of artificial materials with unique properties. Such combinations are used in the design of field-effect transistors (FETs),[10–16] which are useful to overcome the limitations of Si technologies by achieving small channel geometries. Among these, FETs based on MoS_2 have been attracting attention due to low sub-threshold swing values and high on/off current ratios.[10,11] Although MoS_2 shows extraordinary results in FETs, the selection of a gate insulator greatly affects the performance of such devices. It is reported that materials such as SiO_2 or Al_2O_3 expose various problems in such systems due to their amorphous phase and numerous defects in their crystal structures.[17,18] In order to overcome such problems, a well-known single-layer insulator hexagonal boron nitride (*h*-BN) with a wide bandgap of 5.765 eV[19] is employed in numerous FET structures.[20–23] Although there are promising results, the small out-of-plane dielectric constant of *h*-BN that deteriorates the electronic transport properties[24,25] and band offset with similar VBM levels[26] limits the performance of the FET structures. In addition, it is reported that in MoS_2/*h*-BN heterostructures, the presence of intrinsic defects in the *h*-BN layer creates defect states either inside the bandgap or close to the band edge of MoS_2,[20] which could trap the carriers in the devices. Therefore, the competitive 2D insulator to serve as the dielectric layer of MoS_2-based FETs remains to be explored.

Calcium fluoride (CaF_2) has been investigated in various fields. Due to its transparency over a wide spectrum of optical frequencies, CaF_2 is an important material in infrared spectroscopy.[27–29] Applications of CaF_2 extend to a wide range of areas such as laser architecture[30,31] and dentistry.[32,33] Encouraged by such promising results in various fields, thin films of CaF_2 have been studied since the 1990s.[34–36] It is reported that CaF_2 thin films can be used for superlattice,[37] diode,[38] chemical sensors,[39] and transistors.[34] Most recently, the CaF_2 sheet with about 2 nm thickness is used in the design of a

Published under an exclusive license by AIP Publishing

competitive FET based on bilayer MoS_2.[26,40] Low subthreshold swings value of 90 mV dec^{-1} and high on/off current ratios up to 10^7 were realized. In previous works, single-layer CaF_2 in the 1T structure is theoretically predicted, and its dynamical stability and insulating characteristic with a wide bandgap of 9.49 eV[41,42] are reported. Given the excellent properties of two-dimensional CaF_2, it is expected to be an appealing material in nanoscale heterojunction and substrate applications that complements the widely used *h*-BN.

In this article, using *ab initio* calculations, the monolayer MoS_2 heterostructures with monolayer CaF_2 are predicted, and it is revealed that type-I heterojunction is formed[43] with large band offsets. Furthermore, the effects of intrinsic fluorine and calcium vacancies on the CaF_2 layer and the CaF_2/MoS_2 heterostructure are investigated. It is found that in single-layer CaF_2, V_F introduces a deep level below the CBM, whereas V_{Ca} introduces a shallow level at the VBM. In both cases, spin polarization around the vacancy sites is observed. In CaF_2/MoS_2 heterostructures, the electron or hole on V_F or V_{Ca} defect states will transfer from CaF_2 to MoS_2 due to the large band offset, and the spin polarization vanishes. Nevertheless, there are no defect states inside the gap or around the band edge of MoS_2, and the electronic properties of monolayer MoS_2 is almost intact. Thus, CaF_2 can have potential applications for the dielectric layer of MoS_2-based FETs.

This article is organized as follows: In Sec. II, the details of the computational method and the simulations are given. The results are given in Sec. III and the regarding discussion is supplied about the work in three parts. In Sec. III A, the behavior of calcium and fluorine vacancies in 1T-CaF_2 crystals, in Sec. III B the pure CaF_2/MoS_2 heterostructure, and in Sec. III C the V_F and V_{Ca} defects in the CaF_2/MoS_2 heterostructure are discussed. The results are concluded in Sec. IV.

II. COMPUTATIONAL METHOD

The calculations have been performed using density functional theory (DFT) within the Vienna *ab initio* simulation package (VASP).[44,45] The projected augmented wave (PAW) potential[46] is used to describe the ion and core electrons. The exchange-correlation functional is treated by the generalized gradient approximation (GGA) of Perdew–Burke–Ernzerhof (PBE),[47] and the van der Waals (vdW) corrections are taken into account by the D3 scheme of Grimme.[48] The kinetic energy cutoff of the plane-wave basis set is 600 eV, and the geometries are optimized with the conjugate gradient method. The criteria for the total energy convergency during self-consistent calculation is 10^{-5} eV. Spin–orbit interactions are taken into account in the electronic band structure calculations.

The single-layer CaF_2 is simulated by a $(2, 4) \times (6, -2) \times 1$ supercell [the lattice parameter of its primitive cell is $a_{CaF_2} = 3.60$ Å, as shown in Fig. 1(a)] to discuss the behavior of defects. We model the CaF_2/MoS_2 heterostructures by stacking the above CaF_2 layer on top of a $6 \times 6 \times 1$ supercell of single-layer MoS_2 ($a_{MoS_2} = 3.16$ Å). The lattice mismatch between the two layers is about 0.34 %, and it consists of 192 atoms in the simulation cell. When introducing one defect per cell, we optimize the atomic positions until the remaining atomic forces are less than 0.01 eV/Å and fix the cell parameters at the value of 18.96 Å of the MoS_2 supercell. A vacuum layer larger than 20 Å is also introduced to minimize interactions between periodic images.

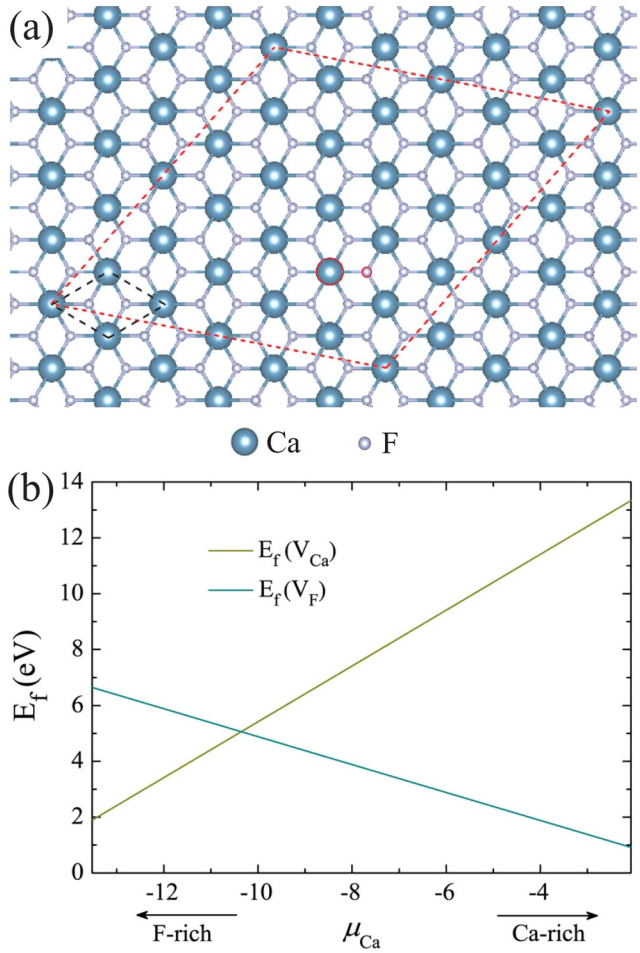

FIG. 1. (a) Crystal structures of pristine 1T-CaF_2. Its primitive cell is given by the black dashed line and the $(2, 4) \times (6, -2) \times 1$ supercell is marked by the red dashed line. The single Ca or F vacancies in the CaF_2 monolayer are marked by red circles. (b) The formation energies of V_{Ca} and V_F defects in CaF_2 as a function of chemical potential μ_{Ca}.

The formation energies (E_f) of vacancies defects (V_i) in CaF_2 are calculated as follows:[49]

$$E_f(V_i) = E(V_i) - E(CaF_2) + \Sigma_i n_i \mu_i, \tag{1}$$

where $E(CaF_2)$ and $E(V_i)$ are the total energies of the perfect and defective systems of CaF_2, n_i is the number of vacant atoms of type i, and μ_i is the chemical potential of element i. One can define the relative chemical potential $\triangle\mu_i = \mu_i - \mu_i^0$ (μ_i^0 is the chemical potential of element i in its most stable elemental phase), which

Published under an exclusive license by AIP Publishing

meet the boundary conditions

$$\begin{aligned} \triangle\mu_{\mathrm{Ca}} &\leq 0, \\ \triangle\mu_{\mathrm{F}} &\leq 0, \\ \triangle\mu_{\mathrm{Ca}} + 2\triangle\mu_{\mathrm{F}} &= \triangle H_f(\mathrm{CaF_2}), \end{aligned} \tag{2}$$

where $\triangle H_f(\mathrm{CaF_2})$ is the formation enthalpy of CaF_2. Thus, we obtain the formation energies of V_i defects in CaF_2 as a function of chemical potential μ_{Ca} and allowed range of μ_{Ca},

$$\begin{aligned} E_f(V_{\mathrm{Ca}}) &= E(V_{\mathrm{Ca}}) - E(CaF_2) + \mu_{\mathrm{Ca}}, \\ E_f(V_{\mathrm{F}}) &= E(V_{\mathrm{F}}) - \frac{E(\mathrm{CaF_2}) + \mu_{\mathrm{Ca}}}{2}, \\ \triangle H_f(\mathrm{CaF_2}) + \mu^0_{\mathrm{Ca}} &\leq \mu_{\mathrm{Ca}} \leq \mu^0_{\mathrm{Ca}}. \end{aligned} \tag{3}$$

III. RESULTS AND DISCUSSION

A. The behavior of calcium and fluorine vacancies in 1T-CaF_2 crystals

The native defects are always generated during crystal growth and such imperfections in the periodic lattice structure directly lead to the alteration of the electronic and magnetic properties of the system more or less. Therefore, investigation of defects is of great importance. We first investigate the structural and electronic behavior of the native vacancy defects, namely, V_{Ca} and V_{F}, in the 1T-CaF_2 crystal.

When a single Ca vacancy is introduced in the CaF_2 monolayer [Fig. 1(a)], its nearby F atoms move away from the vacancy site after structural relaxation, resulting in a 0.05 Å reduction of Ca–F bond length compared with the defect-free case. This is possibly caused by Coulomb repulsion between these negatively charged F atoms. The formation energy of V_{Ca} as a function of Ca chemical potential is shown in Fig. 1(b), and the value is about 13.34 eV under Ca-rich condition, smaller than the value of 13.75 eV in crystalline CaF_2.[50] Under F-rich condition, the formation energy decreases to 2.07 eV. The density of states (DOS) of V_{Ca} is plotted in Fig. 2(a). It is seen that V_{Ca} does not introduce the in-gap defect state. Moreover, while the up-spin states in the valence band are fully occupied, the down-spin states near the VBM are partially unoccupied. These states are mainly contributed by fluorine atoms around vacancy [Fig. 2(c)]. Therefore, the calcium vacancy introduces a magnetic moment of $2\mu_B$ with spin polarization mainly localized on fluorine atoms surrounding the vacancy [Fig. 2(b)].

Meanwhile, the fluorine vacancy causes the slight displacement of calcium atoms around vacancy. The formation energy is about 6.64 eV under F-rich condition and 0.92 eV under Ca-rich condition (Fig. 1). Overall, the formation energy of V_{F} is smaller than that of V_{Ca}, except for the F-rich region ($\mu < -10.49$ eV), suggesting that the V_{F} defect is more likely to exist in the CaF_2 layer. Experiments showed that the major defect in the CaF_2 crystal is the V_{F}-related anti-Frenkel defect.[51] Moreover, other theoretical calculations also reveal higher formation energy of Ca vacancies compared to F vacancies.[50,52] These observations are consistent with our results. The corresponding density of states is shown in Fig. 3. V_{F} introduces a defect level inside the bandgap, with its spin-up component fully occupied while the spin-down component empty. Thus, we obtain a spin-polarized ground state with a magnetic moment of $1\mu_B$ and the spin polarization is localized at the position of vacancy [Fig. 3(a)]. The charge density distribution of the defect levels is presented in Figs. 3(c) and 3(d), and it indicates that the defect levels are mainly contributed by F vacancies.

When the multiple point defects exist in the structures, it will exhibit ferromagnetic (FM) and anti-ferromagnetic (AFM) states. Here, magnetism caused by F defect pair is investigated by comparing defect formation energies as a function of neighboring distance. The second F defect is formed by removing the F atom at the sites displayed in Fig. 4(a). In single CaF_2 layers with F defect pairs, FM and AFM phases exhibit $2\mu_B$ and $0\mu_B$ net magnetic moments, respectively, which are reflected in the corresponding spin densities presented in Figs. 4(b)–4(f). The formation energy of the second F vacancy at different sites under the F-rich and the Ca-rich conditions is shown in Fig. 4(g). It is obtained that second F vacancy located in site 1 has the lowest formation energy in the AFM state and highest energy in the FM state, and the corresponding energy difference is 145 meV [Figs. 4(g) and 4(h)]. In the AFM case, the formation energies of 6.53 eV under the F-rich condition and 0.81 eV under the Ca-rich condition are also smaller than that of the single V_{F} case, indicating that the V_{F} defects tend to form neighboring pairs in the AFM state. With the increasing distance between F vacancies, the energy differences between FM and AFM states decrease (17, 4, and 1 meV at site 2, 3, and 4, respectively). This phenomenon is caused by attraction (repulsion) forces between neighboring defects in the AFM (FM) phase. Furthermore, the magnetic ground state caused by defect pair formation remains as AFM. When the second F defect is located at site 5, the energy difference between FM and AFM phases becomes negligible, indicating that the interaction between neighboring defects is very weak with large enough distance. We have also analyzed the DOS of a single V_{F} and a neighboring V_{F} pair and found their defect state energy is quite similar, and the difference is less than 0.08 eV. For simplicity, we will use a single V_{F} model in heterostructure calculation.

B. Pure CaF_2/MoS_2 heterostructure

Now we discuss the properties of the defect-free heterostructure of a CaF_2 monolayer stacked on the MoS_2 monolayer. After structural relaxation, the average distance between fluorine and sulfur atomic layers in the interstitial region is about 3.06 Å, as shown in Fig. 5. The Ca–F and Mo–S bond lengths are 2.285 and 2.408 Å, respectively.

To clearly understand the electronic properties of the CaF_2/MoS_2 heterostructure, we first give the electronic band structures of isolated layers of CaF_2 and MoS_2 (Fig. 6). With PBE-D3 calculations, we obtain an indirect bandgap of 7.09 eV for CaF_2, compared with other theoretical value of 7.17 eV.[41] For MoS_2, a direct bandgap of 1.66 eV is given, which is close to the other calculated value of 1.75 eV,[20] and the valance top and the conduction bottom are located at the K point. To identify the type of CaF_2/MoS_2

Published under an exclusive license by AIP Publishing

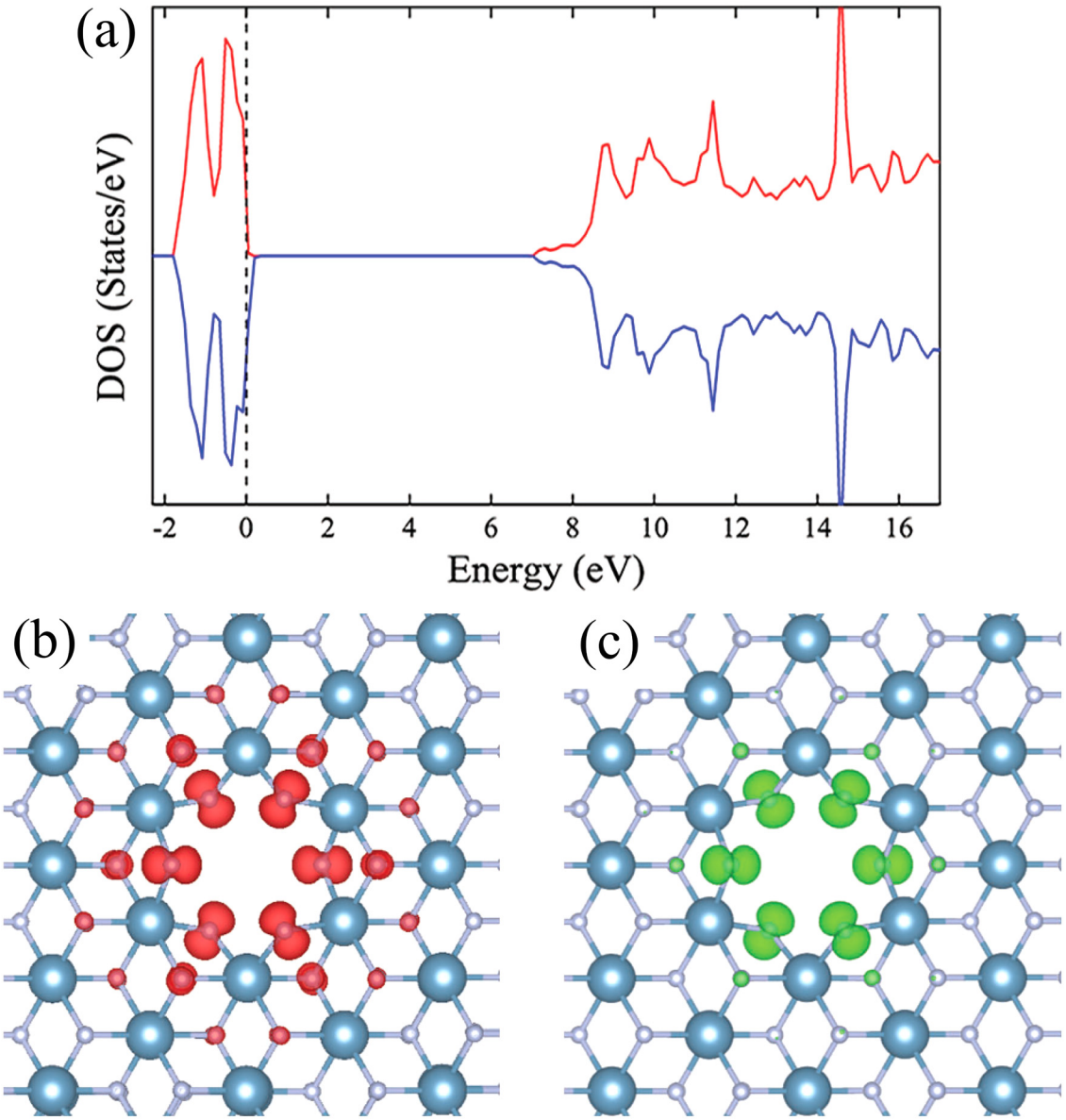

FIG. 2. (a) The spin-polarized density of states and (b) spin density for the V_{Ca} defect in the CaF_2 monolayer. The fermi energy in (a) is set at zero. Here, red color in the spin density plot represents the spin-up channel, and there is no net spin-down contribution. (c) The sum of the partial charge densities (in green) for the states in the energy range of 0–0.5 eV (as well as in other relevant figures). It is contributed by unoccupied spin-down states. The isosurface level of charge density is set to 0.002 e/Bohr^3.

heterostructure, we compare the band alignment of CaF_2 and MoS_2 by aligning the vacuum levels and find that the valence-band edge has lower energy in CaF_2 than that of MoS_2 while the conduction-band edge shows a opposite trend [Fig. 6(b)], suggesting CaF_2/MoS_2 to be a type I (straddling gap) heterojunction.[43] If Anderson's rule is applicable (i.e., the charge transfer and interlayer interaction are negligible), then the valence band offset (VBO) can be estimated as 3.01 eV, and the conduction band offset (CBO) can be estimated as 2.42 eV. Using the hybrid functional HSE06 method,[53] the valance and conduction-band offsets of CaF_2 and MoS_2 increase by 1.03 and 0.29 eV [Fig. 6(c)]. According to the HSE06 calculation, the bandgap of monolayer MoS_2 is 2.31 eV. We also performed G_0W_0 calculation and found a larger quasi-particle gap of 2.95 eV, consistent with previous studies.[54] On the other

Published under an exclusive license by AIP Publishing

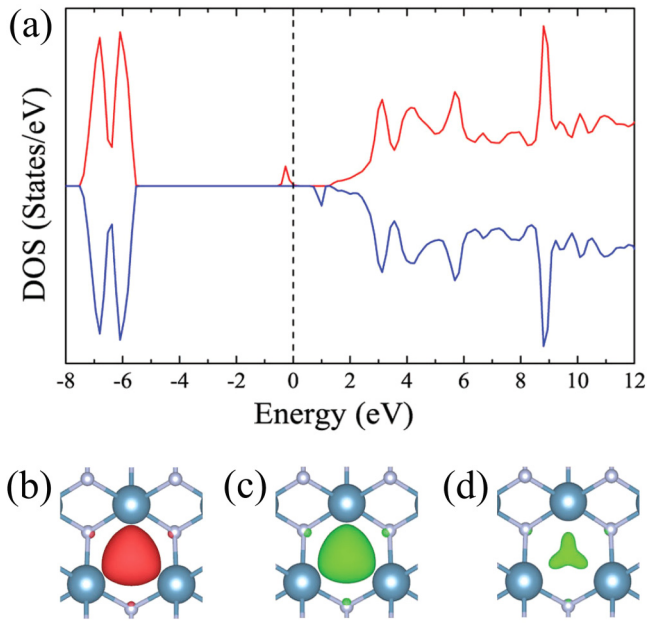

FIG. 3. (a) The spin-polarized density of states and (b) spin density for the V_F defect in the CaF_2 monolayer. The fermi energy in (a) is set at zero. Here, red color in the spin density plot represents the spin-up channel, and there is no net spin-down contribution. (c)–(d) The sum of the partial charge densities (in green) in the range of (c) −1 to 0 eV and (d) 0.5 to 1.1 eV. They are contributed by isolated occupied spin-up states and unoccupied spin-down states, respectively. The isosurface level is set to 0.0055 e/Bohr^3.

hand, the calculated G_0W_0 gap for monolayer CaF_2 is 12.48 eV, which is 3.42 eV larger than the HSE06 result. Thus, the band offset between CaF_2 and MoS_2 is likely to be underestimated even by HSE06. Nevertheless, the type of band alignment and the large band offset values should not be qualitatively affected by the choice of PBE, HSE06, or G_0W_0. In addition, it should have no significant influence on our prediction after two subsystems' combination since the corresponding band offset is large enough.

To further verify the type-I band offset, the partial density of states (PDOS) of the CaF_2/MoS_2 heterostructure is calculated using PBE-D3, as shown in Fig. 7. The result confirmed the predicted type-I character of the CaF_2/MoS_2 heterostructure. Through the band alignment, we obtain that the eigenvalues of the band edges of CaF_2 relative to that of MoS_2 move about 0.3 eV to higher energy after the formation of the heterostructure. Such a shift indicates the formation of a small interface dipole due to charge transfer from MoS_2 to CaF_2. Nevertheless, the VBO (2.60 eV) and the CBO (2.75 eV) remain large. To explore possible hybridization-induced self-energy correction, we also performed HSE06 calculation for the MoS_2/CaF_2 heterstructure supercell and found that the VBO and CBO are 4.03 and 3.05 eV, which is only slightly modified compared to the prediction from Anderson's rule [Fig. 6(c)]. Considering the underestimation of bandgap due to the use of PBE and HSE06, the actual band offsets would be even higher. It is interesting to note that with either PBE or HSE06, we observed an ∼0.07 eV reduction in the bandgap of MoS_2. The gap reduction could possibly be contributed by the dielectric screening effect[55] of the CaF_2, and such effect is typically a few tens of meV for TMDs.[56] Experimentally, *h*-BN is often adopted as the dielectric layer of electronic devices based on 2D materials. However, although *h*-BN also has a type-I band offset with MoS_2,[20,57] their VBO is quite small (∼0.1 eV), which can lead to large gate leakage currents. Therefore, on the basis of band offset, CaF_2 is more suitable to serve as the dielectric layer of MoS_2-based transistors than *h*-BN.

C. The behavior of V_{Ca} and V_F defects in CaF_2/MoS_2 heterostructure

Intrinsic defect properties of the dielectric layer in transistors can greatly affect the device performance. In this section, we investigate the effects of V_{Ca} and V_F defects on CaF_2/MoS_2 heterostructures. Considering the two layers of F atoms in the heterostructure, there could be two types of V_F. One is located at the heterostructure interface (denoted as V_F-d), and the other one is located at the outer surface (denoted as V_F-u). The removal of a fluorine atom from the CaF_2 layer leads to a significant change for geometry. As the fluorine and calcium atoms around vacancies move outward relative to the position of vacancy, they also move toward the interstitial region between the layers due to the existence of the MoS_2 layer. The Ca–F bond length is 0.07 Å longer for V_F-u defect than that of defect-free heterostructure defect while 0.04 Å longer for V_F-d defect. In the case of V_{Ca} defect, geometry distortion is smaller. The Ca–F bond lengths around the vacancies are about 0.1 Å shorter than the defect-free case, similar to the V_{Ca} defect in the isolated CaF_2 layer.

Figure 8 plots the density of states for V_F-u, V_F-d, and V_{Ca} defects in the CaF_2/MoS_2 heterostructure. With the presence of MoS_2 layer, the defect state close to the conduction-band edge caused by fluorine vacancy in the CaF_2 layer vanishes [Figs. 8(a) and 8(b)], and spin polarization also disappears. The Fermi levels in the V_F-u and V_F-d cases are both located at the conduction-band edge of the MoS_2 layer, and the valence-band offset increases by 0.41 eV for V_F-u defect and 0.17 eV for V_F-d defect compared to the defect-free case. According to Fig. 3(a), the V_F defect level is about 1 eV lower than the CBM of CaF_2, while the CBO between CaF_2 and MoS_2 is 2.75 eV. Hence, the defect level is much higher than the CBM of MoS_2, and the electron occupying the defect level in CaF_2 will transfer to the conduction band of MoS_2, with the Fermi level shifted to the conduction band edge of MoS_2. Such a defect-induced indirect doping is also observed in the MoS_2/BN heterostructure.[20] The situation for V_{Ca} is similar [Fig. 8(c)], except for that the transferred carrier is hole. Due to the large VBO between MoS_2 and CaF_2, the Fermi level crosses the valence band edge of MoS_2, and four fully occupied defect states occur above the valence-band top of the CaF_2 subsystem. There is also no magnetism. Moreover, the band offset is modified by Ca vacancy, with about 1.12 eV reduction (increase) in VBO (CBO). The charge density of the states for the V_F-u and V_F-d cases at the conduction band below the Fermi level is shown in Figs. 8(d) and 8(e) and that for the V_{Ca} case at the valence band above the Fermi level is shown in Fig. 8(f). It is seen that these states mainly locate on the MoS_2

Published under an exclusive license by AIP Publishing

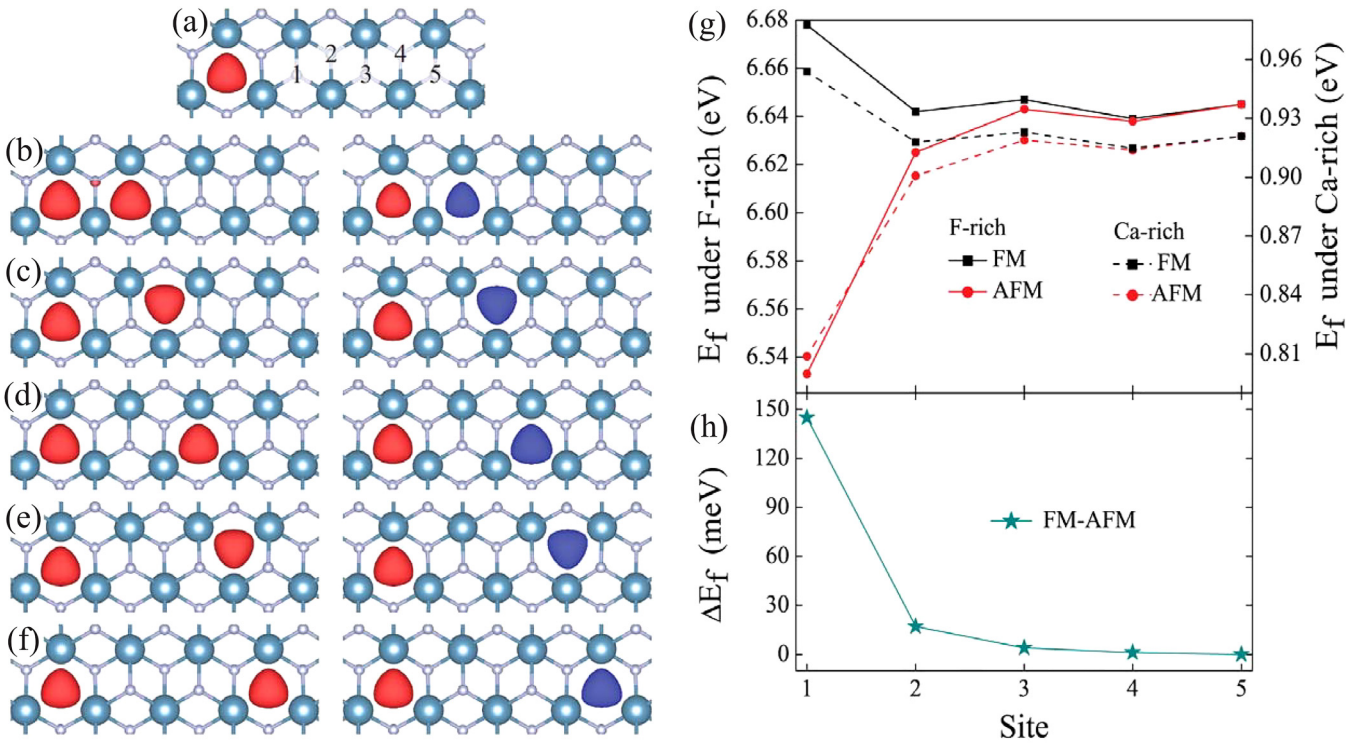

FIG. 4. (a) The possible F vacancy sites 1, 2, 3, 4, and 5 for the formation of defect pair in CaF_2 with single F vacancy. The spin density of F defect pairs with FM and AFM phases where the second F vacancy is located at sites (b) 1, (c) 2, (d) 3, (e) 4, and (f) 5. Red or blue represents spin-up or spin-down channel here. The isosurface level is set to 0.007 e/Bohr^3. (g) The formation energy of second F vacancies under F-rich and Ca-rich conditions and (h) energy differences at five sites.

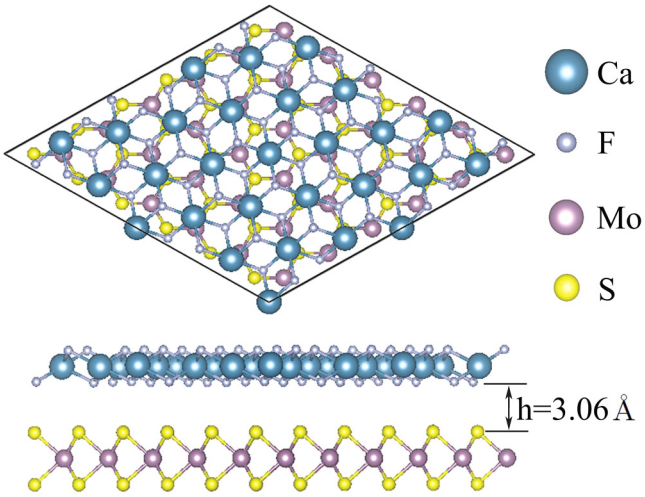

FIG. 5. The top and side views of CaF_2/MoS_2 heterostructure. Its simulated cell is constructed by stacking a (2, 4) × (6, − 2) × 1 supercell of CaF_2 on a 6 × 6 × 1 supercell of MoS_2.

layer and are quite delocalized, leading to the disappearance of magnetism. Previous studies revealed that in the MoS_2/*h*-BN heterostructure, vacancies in *h*-BN creates defect states either close to the band edge of MoS_2 or inside its bandgap;[20] thus, the carrier transport in MoS_2 may be affected by these defect states. In the case of MoS_2/CaF_2 heterostructure, the vacancies in CaF_2 do not introduce defect states inside the gap or around the band edge. Comparing Figs. 7 and 8(a)–8(c), it is seen that when interfaced with defective CaF_2, the DOS of the MoS_2 layer are quite similar to the case in a perfect heterostructure, indicating the effect of vacancies to the electronic structure of the MoS_2 layer is minor. Such a defect insensitivity, combined with a proper band offset, makes CaF_2 a good candidate for the dielectric layer of MoS_2-based transistors.

It is worth to mention that the FET made in experiments consists of ∼2 nm thick CaF_2 and bilayer MoS_2,[26,40] while in our calculation, monolayers are used. To explore the possible thickness effect, we have calculated the band structures of 5-layer CaF_2 and bilayer MoS_2. The bandgap of 5-layer CaF_2 and bilayer MoS_2 is 6.80 and 1.23 eV, which are smaller than our calculated data of monolayer CaF_2 (7.09 eV) and MoS_2 (1.66 eV), respectively. The VBO or CBO between CaF_2 and MoS_2 multi-layers is 2.93 or 2.64 eV, which is

Published under an exclusive license by AIP Publishing

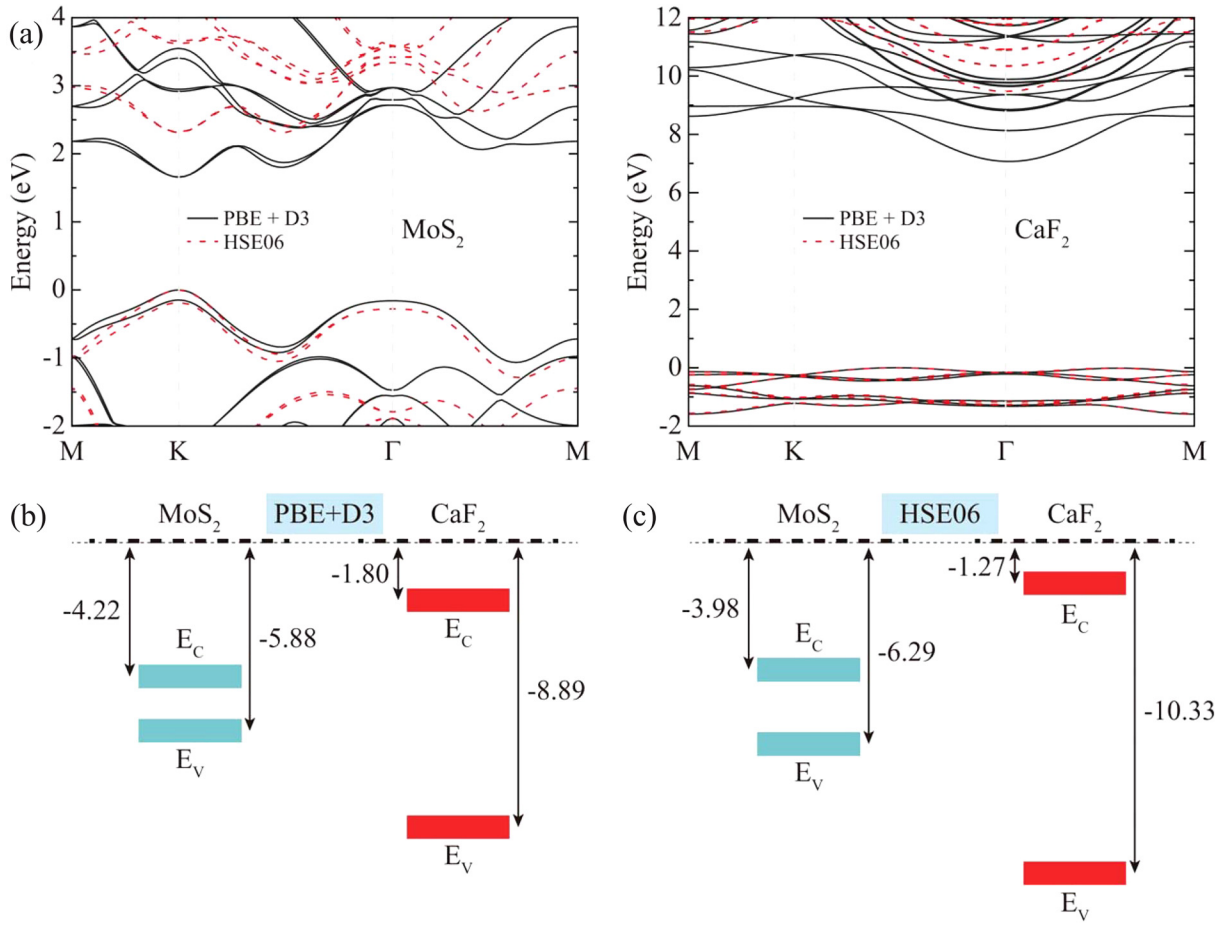

FIG. 6. (a) Electronic band structures of MoS_2 and CaF_2 calculated by PBE-D3 method and HSE06 method[53] with spin–orbital coupling. The bandgap of MoS_2 and CaF_2 is 1.66 and 7.09 eV by PBE-D3 method and 2.31 and 9.06 eV by HSE06 method, respectively. For comparison, the valence-band maximum is set to be zero of energy by shifting the band structures. The band alignment of MoS_2 and CaF_2 using (b) PBE-D3 method and (c) HSE06 method. The vacuum energies are set to zero.

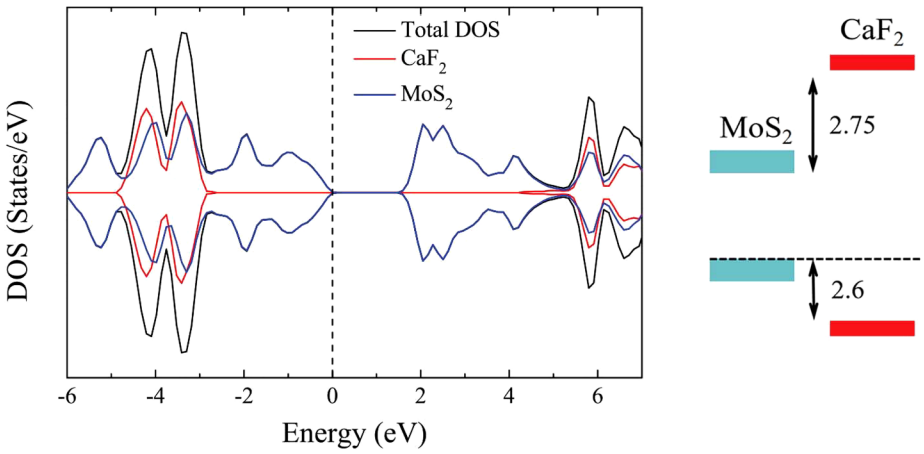

FIG. 7. The spin-resolved partial density of states (PDOS) and band alignment of the CaF_2/MoS_2 heterostructure. The Fermi level is set to zero. The bandgap of MoS_2 and CaF_2 in the heterostructure is 1.59 and 6.96 eV by the PBE-D3 method, respectively.

Published under an exclusive license by AIP Publishing

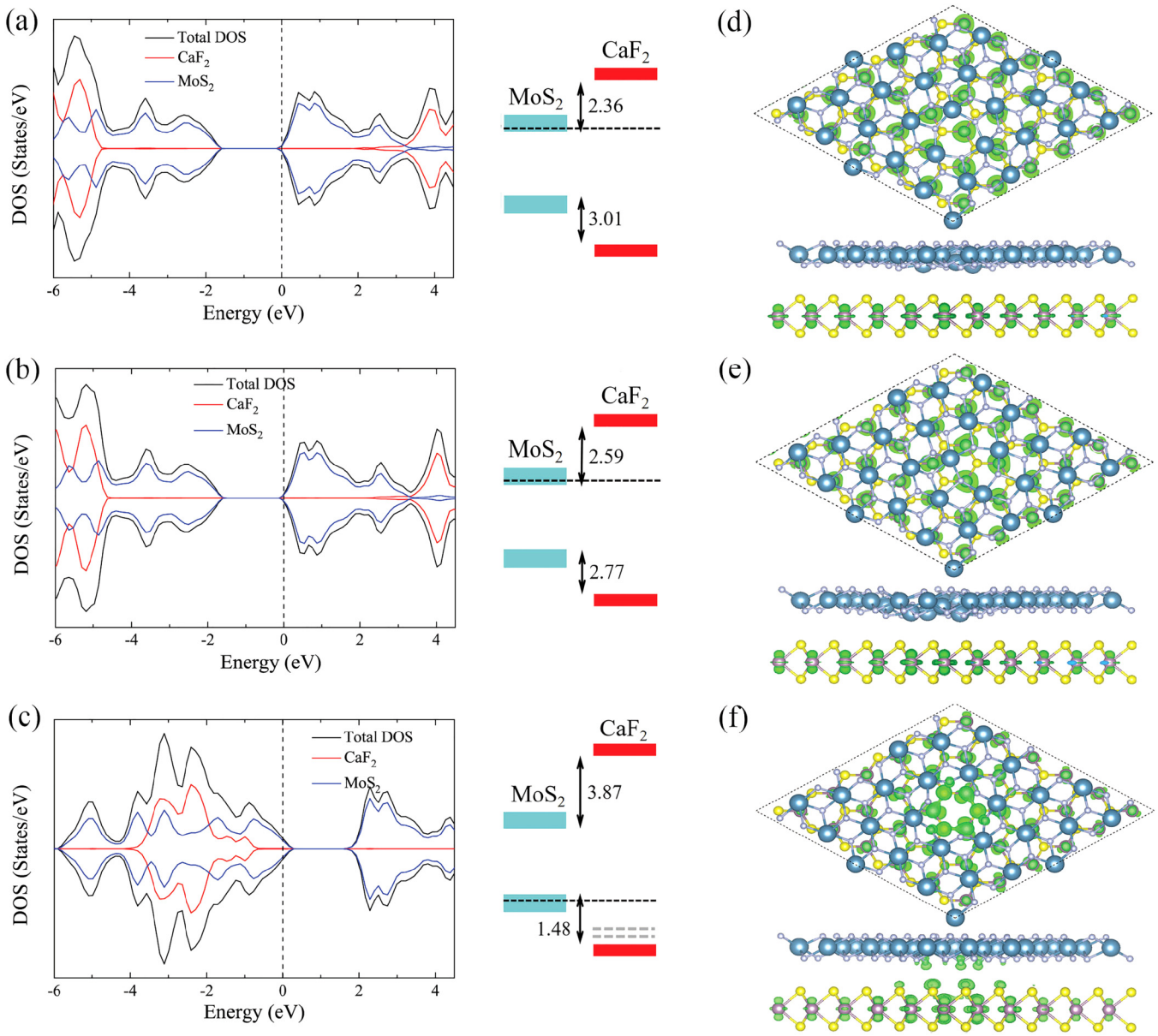

FIG. 8. The spin-resolved partial density states and band alignment of (a) V_F-u, (b) V_F-d, and (c) V_{Ca} defects in CaF_2/MoS_2 heterostructures. The Fermi energy is located at zero with a black dashed line. The gray dashed line in (c) denotes the defect levels. The top and side views of band-decomposed charge density distributions of the conduction band in the energy range of −0.5 to 0 eV for (d) V_F-u and (e) V_F-d defects and (f) the valence band in the energy range of 0–0.5 eV for V_{Ca} defect. The isosurface level is set to 0.00007 e/Bohr^3 in (d) and (e) and 0.001 e/Bohr^3 in (f).

close to the value of 3.01 or 2.42 eV for the monolayer case. Therefore, our results remain valid for systems using thicker films. Moreover, the control of a FET is achieved through a gate electric field (the magnitude is typically less or comparable to 0.1 V/Å). To explore the electric field effect, we have calculated the properties of the CaF_2/MoS_2 monolayer heterostructure under the electric field of 0.1 and −0.1 V/Å. It is found that the change in the VBO and CBO is within ∼0.1 eV. Therefore, at an experimentally achievable strength, the gate electric field should have minor effect on the electronic states on the CaF_2/MoS_2 heterostructure.

Published under an exclusive license by AIP Publishing

IV. CONCLUSION

In conclusion, the structural and electronic properties of the intrinsic vacancies in an isolated CaF_2 layer and CaF_2/MoS_2 heterostructures are investigated from first-principles calculations. The removal of fluorine or calcium atom from the isolated CaF_2 layer induces spin polarization around vacancies with magnetic moment of $1\mu_B$ or $2\mu_B$, respectively. V_{Ca} introduces a shallow defect level close to the VBM, whereas V_F introduces a deep level below the CBM. Overall, V_F has a relatively lower formation energy than V_{Ca}, except for the extremely Ca-rich case. Thus, V_F should be dominant in CaF_2. The magnetic coupling between the fluorine vacancy pair is also studied, and it is found that the nearest-neighbor pair with AFM configuration is favorable due to the lower formation energy. The band offset between CaF_2 and MoS_2 is determined to be type-I, with large CBO and VBO. With the presence of vacancies in CaF_2, the type-I band offset is maintained. The electron or hole on the defect states will transfer from CaF_2 to MoS_2 due to the large band offset, and spin polarization vanishes. Nevertheless, there are no defect states inside the gap or around the band edge of MoS_2, and the electronic properties of MoS_2 are almost intact. Compared with *h*-BN that has a small VBO with MoS_2 and could introduce in-gap defect states, CaF_2 can be a good candidate to serve as the dielectric layer of MoS_2-based transistors.

ACKNOWLEDGMENTS

This work was supported by the Postdoctoral Science Foundation of China (Grant No. 2019M650463) and the Natural Science Foundation of China (NSFC) (Grant Nos. 12074029 and U1930402). The authors gratefully acknowledge computational resources provided by TianHe2-JK in CSRC used for the simulations in this work. H.S. acknowledges the financial support from the TUBITAK under Project No. 117F095. H.S. acknowledges support from the Turkish Academy of Sciences under the GEBIP program. H.S. acknowledges the computational resources provided by TUBITAK ULAKBIM, High Performance and Grid Computing Center (TR-Grid e-Infrastructure).

DATA AVAILABILITY

The data that support the findings of this study are available from the corresponding author upon reasonable request.

REFERENCES

[1]J. V. Lauritsen, J. Kibsgaard, S. Helveg, H. Topsøe, B. S. Clausen, E. Lægsgaard, and F. Besenbacher, "Size-dependent structure of MoS_2 nanocrystals," Nat. Nanotech. **2**, 53–58 (2007).

[2]K. F. Mak, C. Lee, J. Hone, J. Shan, and T. F. Heinz, "Atomically thin MoS_2: A new direct-gap semiconductor," Phys. Rev. Lett. **105**, 136805 (2010).

[3]Q. H. Wang, K. Kalantar-Zadeh, A. Kis, J. N. Coleman, and M. S. Strano, "Electronics and optoelectronics of two-dimensional transition metal dichalcogenides," Nat. Nanotech. **7**, 699–712 (2012).

[4]Z. Yin, H. Li, H. Li, L. Jiang, Y. Shi, Y. Sun, G. Lu, Q. Zhang, X. Chen, and H. Zhang, "Single-layer MoS_2 phototransistors," ACS Nano **6**, 74–80 (2012).

[5]I. Kaplan-Ashiri, S. R. Cohen, K. Gartsman, V. Ivanovskaya, T. Heine, G. Seifert, I. Wiesel, H. D. Wagner, and R. Tenne, "On the mechanical behavior of WS_2 nanotubes under axial tension and compression," Proc. Natl. Acad. Sci. U.S.A. **103**, 523–528 (2006).

[6]W. Zhang, C.-P. Chuu, J.-K. Huang, C.-H. Chen, M.-L. Tsai, Y.-H. Chang, C.-T. Liang, Y.-Z. Chen, Y.-L. Chueh, J.-H. He *et al.*, "Ultrahigh-gain photodetectors based on atomically thin graphene-MoS_2 heterostructures," Sci. Rep. **4**, 3826 (2014).

[7]H. Terrones, F. López-Urías, and M. Terrones, "Novel hetero-layered materials with tunable direct band gaps by sandwiching different metal disulfides and diselenides," Sci. Rep. **3**, 1549 (2013).

[8]L. Britnell, R. Gorbachev, R. Jalil, B. Belle, F. Schedin, A. Mishchenko, T. Georgiou, M. Katsnelson, L. Eaves, S. Morozov *et al.*, "Field-effect tunneling transistor based on vertical graphene heterostructures," Science **335**, 947–950 (2012).

[9]S. Bertolazzi, D. Krasnozhon, and A. Kis, "Nonvolatile memory cells based on MoS_2/graphene heterostructures," ACS Nano **7**, 3246–3252 (2013).

[10]Y. Y. Illarionov, K. K. Smithe, M. Waltl, T. Knobloch, E. Pop, and T. Grasser, "Improved hysteresis and reliability of MoS_2 transistors with high-quality CVD growth and Al_2O_3 encapsulation," IEEE Electron. Device Lett. **38**, 1763–1766 (2017).

[11]P. Bolshakov, P. Zhao, A. Azcatl, P. K. Hurley, R. M. Wallace, and C. D. Young, "Improvement in top-gate MoS_2 transistor performance due to high quality backside Al_2O_3 layer," Appl. Phys. Lett. **111**, 032110 (2017).

[12]J. Kang, W. Liu, and K. Banerjee, "High-performance MoS_2 transistors with low-resistance molybdenum contacts," Appl. Phys. Lett. **104**, 093106 (2014).

[13]K. K. Smithe, S. V. Suryavanshi, M. Munoz Rojo, A. D. Tedjarati, and E. Pop, "Low variability in synthetic monolayer MoS_2 devices," ACS Nano **11**, 8456–8463 (2017).

[14]W. Liao, W. Wei, Y. Tong, W. K. Chim, and C. Zhu, "Electrical performance and low frequency noise in hexagonal boron nitride encapsulated $MoSe_2$ dual-gated field effect transistors," Appl. Phys. Lett. **111**, 082105 (2017).

[15]L. Yang, K. Majumdar, H. Liu, Y. Du, H. Wu, M. Hatzistergos, P. Hung, R. Tieckelmann, W. Tsai, C. Hobbs *et al.*, "Chloride molecular doping technique on 2D materials: WS_2 and MoS_2," Nano Lett. **14**, 6275–6280 (2014).

[16]A. Prakash and J. Appenzeller, "Bandgap extraction and device analysis of ionic liquid gated WSe_2 Schottky barrier transistors," ACS Nano **11**, 1626–1632 (2017).

[17]Y.-Y. Liu, F. Liu, R. Wang, J.-W. Luo, X. Jiang, R. Huang, S.-S. Li, and L.-W. Wang, "Characterizing the charge trapping across crystalline and amorphous $Si/SiO_2/HfO_2$ stacks from first-principle calculations," Phys. Rev. Appl. **12**, 064012 (2019).

[18]Y.-Y. Liu, F. Zheng, X. Jiang, J.-W. Luo, S.-S. Li, and L.-W. Wang, "Ab initio investigation of charge trapping across the crystalline-Si–amorphous-SiO_2 interface," Phys. Rev. Appl. **11**, 044058 (2019).

[19]K. Watanabe, T. Taniguchi, and H. Kanda, "Direct-bandgap properties and evidence for ultraviolet lasing of hexagonal boron nitride single crystal," Nat. Mater. **3**, 404–409 (2004).

[20]R. Gillen, J. Robertson, and J. Maultzsch, "Indirect doping effects from impurities in MoS_2/h-BN heterostructures," Phys. Rev. B **90**, 075437 (2014).

[21]H. Jeong, S. Bang, H. M. Oh, H. J. Jeong, S.-J. An, G. H. Han, H. Kim, K. K. Kim, J. C. Park, Y. H. Lee *et al.*, "Semiconductor–insulator–semiconductor diode consisting of monolayer MoS_2, h-BN, and GaN heterostructure," ACS Nano **9**, 10032–10038 (2015).

[22]W. Zan, W. Geng, H. Liu, and X. Yao, "Electric-field and strain-tunable electronic properties of MoS_2/h-BN/graphene vertical heterostructures," Phys. Chem. Chem. Phys. **18**, 3159–3164 (2016).

[23]C. H. Sharma and M. Thalakulam, "Split-gated point-contact for electrostatic confinement of transport in MoS_2/h-BN hybrid structures," Sci. Rep. **7**, 735 (2017).

[24]R. Geick, C. Perry, and G. Rupprecht, "Normal modes in hexagonal boron nitride," Phys. Rev. **146**, 543 (1966).

[25]A. Laturia, M. L. Van de Put, and W. G. Vandenberghe, "Dielectric properties of hexagonal boron nitride and transition metal dichalcogenides: From monolayer to bulk," npj 2D Mater. Appl. **2**, 6 (2018).

[26]Y. Y. Illarionov, A. G. Banshchikov, D. K. Polyushkin, S. Wachter, T. Knobloch, M. Thesberg, L. Mennel, M. Paur, M. Stöger-Pollach,

Published under an exclusive license by AIP Publishing

A. Steiger-Thirsfeld *et al.*, "Ultrathin calcium fluoride insulators for two-dimensional field-effect transistors," Nat. Electron. **2**, 230–235 (2019).
[27]R. Adato and H. Altug, "In-situ ultra-sensitive infrared absorption spectroscopy of biomolecule interactions in real time with plasmonic nanoantennas," Nat. Commun. **4**, 2154 (2013).
[28]H. Yang, S. Yang, J. Kong, A. Dong, and S. Yu, "Obtaining information about protein secondary structures in aqueous solution using Fourier transform IR spectroscopy," Nat. Protoc. **10**, 382–396 (2015).
[29]C. Lecaplain, C. Javerzac-Galy, M. L. Gorodetsky, and T. Kippenberg, "Mid-infrared ultra-high-Q resonators based on fluoride crystalline materials," Nat. Commun. **7**, 13383 (2016).
[30]A. Lucca, M. Jacquemet, F. Druon, F. Balembois, P. Georges, P. Camy, J.-L. Doualan, and R. Moncorgé, "High-power tunable diode-pumped Yb^3+: CaF_2 laser," Opt. Lett. **29**, 1879–1881 (2004).
[31]M. S. Akchurin, T. Basiev, A. Demidenko, M. Doroshenko, P. Fedorov, E. Garibin, P. Gusev, S. Kuznetsov, M. Krutov, I. Mironov *et al.*, "CaF_2: Yb laser ceramics," Opt. Mater. **35**, 444–450 (2013).
[32]L. Sun and L. C. Chow, "Preparation and properties of nano-sized calcium fluoride for dental applications," Dent. Mater. **24**, 111–116 (2008).
[33]H. H. Xu, J. L. Moreau, L. Sun, and L. C. Chow, "Strength and fluoride release characteristics of a calcium fluoride based dental nanocomposite," Biomaterials **29**, 4261–4267 (2008).
[34]T. Smith III, J. M. Phillips, W. Augustyniak, and P. Stiles, "Fabrication of metal-epitaxial insulator-semiconductor field-effect transistors using molecular beam epitaxy of CaF_2 on Si," Appl. Phys. Lett. **45**, 907–909 (1984).
[35]L. Schowalter, R. Fathauer, R. Goehner, L. Turner, R. DeBlois, S. Hashimoto, J.-L. Peng, W. Gibson, and J. Krusius, "Epitaxial growth and characterization of CaF_2 on Si," J. Appl. Phys. **58**, 302–308 (1985).
[36]N. Senguttuvan, M. Aoshima, K. Sumiya, and H. Ishibashi, "Oriented growth of large size calcium fluoride single crystals for optical lithography," J. Cryst. Growth **280**, 462–466 (2005).
[37]S. Suturin, S. Basun, S. Gastev, J. Langer, R. Meltzer, and N. Sokolov, "Optical detection of electron transfer through interfaces in CaF_2: Eu–CdF_2 SLs," Appl. Surf. Sci. **162**, 474–478 (2000).
[38]M. Watanabe, T. Funayama, T. Teraji, and N. Sakamaki, "CaF_2/CdF_2 double-barrier resonant tunneling diode with high room-temperature peak-to-valley ratio," Jpn. J. Appl. Phys. **39**, L716 (2000).
[39]J. W. Fergus, "The application of solid fluoride electrolytes in chemical sensors," Sens. Actuators B **42**, 119–130 (1997).
[40]Y. Y. Illarionov, A. G. Banshchikov, D. K. Polyushkin, S. Wachter, T. Knobloch, M. Thesberg, M. I. Vexler, M. Waltl, M. Lanza, N. S. Sokolov *et al.*, "Reliability of scalable MoS_2 FETs with 2 nm crystalline CaF_2 insulators," 2D Mater. **6**, 045004 (2019).
[41]M. Baskurt, J. Kang, and H. Sahin, "Octahedrally coordinated single layered CaF_2: Robust insulating behaviour," Phys. Chem. Chem. Phys. **22**, 2949–2954 (2020).
[42]M. Baskurt, M. Yagmurcukardes, F. M. Peeters, and H. Sahin, "Stable single-layers of calcium halides (CaX_2, X = F, CCl, BBr, I)," J. Chem. Phys. **152**, 164116 (2020).
[43]T. Ihn, *Semiconductor Nanostructures: Quantum States and Electronic Transport* (Oxford University Press, 2010).
[44]G. Kresse and J. Hafner, "*Ab initio* molecular dynamics for liquid metals," Phys. Rev. B **47**, 558 (1993).
[45]G. Kresse and J. Furthmüller, "Efficient iterative schemes for ab initio total-energy calculations using a plane-wave basis set," Phys. Rev. B **54**, 11169 (1996).
[46]P. E. Blöchl, "Projector augmented-wave method," Phys. Rev. B **50**, 17953 (1994).
[47]J. P. Perdew, K. Burke, and M. Ernzerhof, "Generalized gradient approximation made simple," Phys. Rev. Lett. **77**, 3865 (1996).
[48]S. Grimme, J. Antony, S. Ehrlich, and H. Krieg, "A consistent and accurate ab initio parametrization of density functional dispersion correction (DFT-D) for the 94 elements H-Pu," J. Chem. Phys. **132**, 154104 (2010).
[49]S.-H. Wei, "Overcoming the doping bottleneck in semiconductors," Comput. Mater. Sci. **30**, 337–348 (2004).
[50]K.-D. Li, H. Xiao, and L. Wang, "Computer simulation study of defect formation and migration energy in calcium fluoride," Nucl. Instrum. Methods Phys. Res. B **266**, 2698–2701 (2008).
[51]R. W. Ure, "Ionic conductivity of calcium fluoride crystals," J. Chem. Phys. **26**, 1363–1373 (1957).
[52]A. M. Ibraheem, M. A. H. Khalafalla, and M. H. Eisa, "First principle calculation of accurate native defect levels in CaF2," Eur. Phys. J. B **90**, 42 (2017).
[53]A. V. Krukau, O. A. Vydrov, A. F. Izmaylov, and G. E. Scuseria, "Influence of the exchange screening parameter on the performance of screened hybrid functionals," J. Chem. Phys. **125**, 224106 (2006).
[54]D. Y. Qiu, F. H. da Jornada, and S. G. Louie, "Optical spectrum of MoS_2: Many-body effects and diversity of exciton states," Phys. Rev. Lett. **111**, 216805 (2013).
[55]K. Noori, N. L. Q. Cheng, F. Xuan, and S. Y. Quek, "Dielectric screening by 2d substrates," 2D Mater. **6**, 035036 (2019).
[56]Y. Xu, C. Horn, J. Zhu, Y. Tang, L. Ma, L. Li, S. Liu, K. Watanabe, T. Taniguchi, J. C. Hone, S. Jian, and K. F. Mak, "Creation of moiré bands in a monolayer semiconductor by spatially periodic dielectric screening," Nat. Mater. **20**, 645–649 (2021).
[57]H.-P. Komsa and A. V. Krasheninnikov, "Electronic structures and optical properties of realistic transition metal dichalcogenide heterostructures from first principles," Phys. Rev. B **88**, 085318 (2013).

Published under an exclusive license by AIP Publishing